Electrochimica Acta, Vol. 38, No. 9, pp. 1289–1300, 1993
Printed in Great Britain.

0013–4686/93 $6.00 + 0.00

FOUR PROBE POLARIZATION TECHNIQUES AND THE APPLICATION TO INVESTIGATIONS OF SOLID-STATE ELECTROCHEMICAL DEVICES

MEILIN LIU,* STEVEN J. VISCO and LUTGARD C. DE JONGHE
Department of Materials Science and Mineral Engineering, University of California and Materials Research Division, Lawrence Berkeley Laboratory, 1 Cyclotron Road, Berkeley, CA 94720, U.S.A.

(*Received* 15 *September* 1992)

Abstract—The application of sequential, bipolar, square-wave, current pulses to a solid-state electrochemical device with two properly positioned reference electrodes, has greatly facilitated the characterization of cell performance. This technique is particularly useful in identifying the rate-limiting step by separation of polarization distributions among cell components. Additional utility of this technique includes fast results and easy data interpretation. In fact, the current pulse sequences can be superimposed on a cell under normal operation to determine the kinetic and transport properties of the electrolyte and electrode materials *in situ* during cell operation.

Key words: four-probe, transient, polyorganodisulfide, solid-state, polymer electrolyte.

NOMENCLATURE

A	electrode area, cm^2
C_{dl}	double layer capacitance, F
c_i	concentration of species i, $mol\,cm^{-3}$
c_i^*	concentration of species i in the bulk phase, $mol\,cm^{-3}$
$c_i(0, t)$	concentration of species i at an interface or surface, $mol\,cm^{-3}$
D_i	diffusion coefficient, $cm^2\,s^{-1}$
F	Faraday's constant, 96,487 C equiv^{-1}
i_0	exchange current density, $A\,cm^{-2}$
i_{dl}	double layer charging or discharging current density, $A\,cm^{-2}$
R	universal gas constant, $8.314\,J\,mol^{-1}\,K^{-1}$
R_{ct}	resistance to charge transfer, Ω
t_i	transference number of species i
T	absolute temperature, K
α_a, α_c	anodic and cathodic transfer coefficients
$\eta(t)$	overpotential at a given time t, V
η_{ct}	overpotential due to charge transfer at steady state, V
$\eta_{ct}(t)$	overpotential due to charge transfer at a given time t, V
$\eta_{mt}(t)$	overpotential due to mass transfer at a given time t, V
$\eta_{mt,i}$	overpotential due to mass transfer of species i, V
τ'	double layer relaxation time constant, dimensionless
τ''	transition time constant for mass transfer, dimensionless

* Current Address: School of Materials Science and Engineering, Georgia Institute of Technology, Atlanta, GA 30332-0245, U.S.A.

1. INTRODUCTION

Solid-state electrochemical devices have found wide spread applications in energy storage and conversion, chemical sensing, electrochromic display and environmental protection. Due to solid-state phenomena, the investigation of these devices frequently involves complications, particularly as the thickness of the electrolyte is reduced and as the devices are operated at lower temperatures, where the effect of interfacial phenomena on cell performance becomes more significant.

Although interfacial phenomena can be studied by impedance spectroscopy and potential sweep techniques, *in situ* investigation of these processes is more useful for effective improvement of cell performance.

This paper introduces techniques for investigations of solid-state electrochemical devices using four potential probes and sequential current pulses. These techniques are particularly effective in determining the rate-limiting component of a cell. With careful experimental design, the kinetic processes occurring at interfaces and transport processes throughout the system can be investigated in detail. In addition, once a rate-limiting component or step is identified, detailed investigation of the component or the step can be further studied using other techniques. The usefulness of the four probe polarization techniques will be demonstrated in studies of cells based on

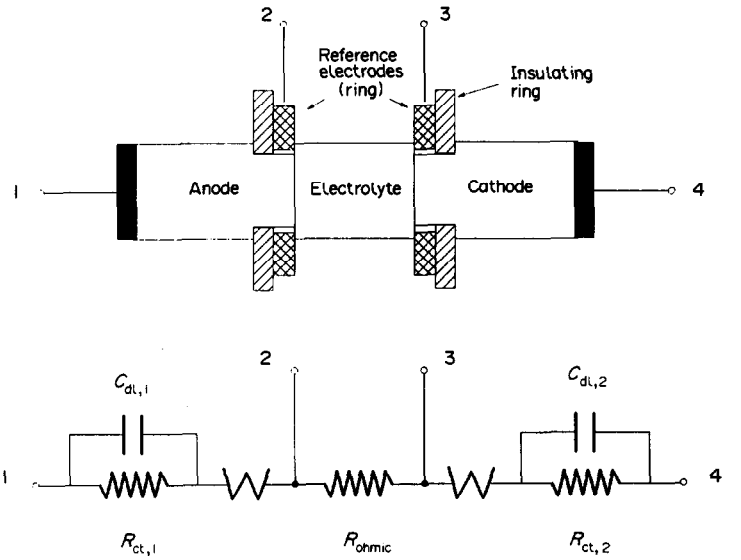

Fig. 1. A schematic view and the corresponding equivalent circuit of a solid-state electrochemical cell with a single layer of electrolyte and four probes.

solid redox polymerization electrodes[1–3] and solid oxide fuel cells[4].

2. EXPERIMENTAL

Shown in Fig. 1 is a schematic view, together with the corresponding equivalent circuit, of a Li/PEO/*srpe* cell with two reference electrodes. A similar cell configuration with two reference electrodes separated by three identical electrolyte layers is shown in Fig. 2. The lithium foil, polyethylene oxide (PEO)-based electrolytes, amorphous PEO (aPEO) and solid redox polymerization electrodes (*srpe*) such as poly-dimercaptothiadiazole (X1) and poly-trithiocyaniric acid (X5) were prepared as described in previous publications[1–3]. Shown in Fig. 3 is a schematic view of a solid oxide fuel cell with two reference electrodes. Tape-cast yttria-stabilized zirconia (YSZ) electrolyte, $La_{0.89}Sr_{0.1}MnO_{3-x}$(LSM) cathode and Ni–$ZrO_2$ cement anode were prepared as described elsewhere[4].

An EG&GPAR 173 potentiostat, interfaced with an IBM-PC/AT through a data translation board,

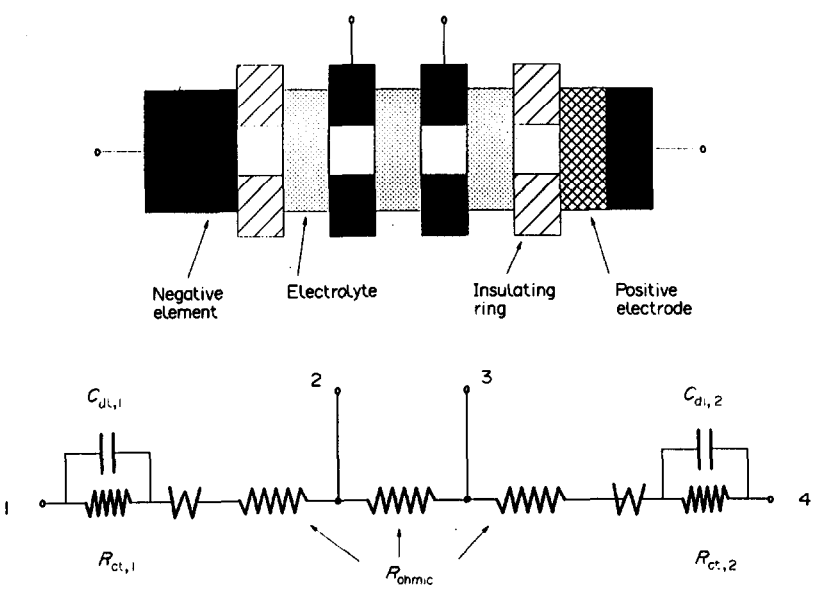

Fig. 2. A schematic view, together with the corresponding equivalent circuit, of a solid-state electrochemical cell with three identical layers of electrolyte and four probes.

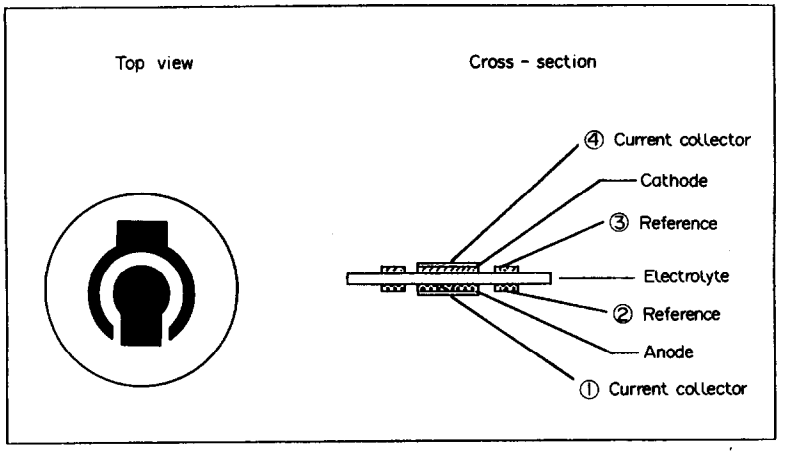

Fig. 3. A schematic view of a solid oxide fuel cell with four probes. The specific electrode pattern and cell configuration were designed for performance isolation of each cell component.

was used to control the current or potential. A program[5] written in Asyst was used to generate current pulses as shown in Fig. 4 and subsequently to acquire potential responses at four probes under each current pulse at $t = \tau_0$. A Schlumberger frequency response analyser 1255 and electrochemical interface 1286, interfaced with an IBM PC/386, were used to measure the impedance of solid-state electrochemical systems in the frequency range from mHz to MHz.

3. ANALYSIS

3.1. *Effect of double layer charging*

Under the assumption that mass transfer is infinitely fast, the potential drop cross an interface, at time t after a constant current I is applied to the interface, can be expressed as

$$\eta(t) = \eta_{ct}\left[1 - \exp\left(-\frac{t}{C_{dl}R_{ct}}\right)\right], \tag{1}$$

where η_{ct} is the charge transfer overpotential, C_{dl} is the double layer capacitance of the interface and R_{ct} is the charge transfer resistance of the interface.

When the current due to double layer charging vanishes ($i_{dl} \to 0$), the applied current approaches the current due to faradaic processes (I_f) and the interfacial overpotential, $\eta(t)$, approaches the steady-state charge transfer overpotential, η_{ct}, which is implicitly related to the applied current, I, as

$$\frac{I}{A} = \frac{I_f}{A} = i_0\left\{\exp\left[\frac{\alpha_a F\eta_{ct}}{RT}\right] - \exp\left[-\frac{\alpha_c F\eta_{ct}}{RT}\right]\right\}, \tag{2}$$

where A is the surface area of the electrode, i_0 is the exchange current density, R is the gas constant, T is the absolute temperature, F is Faraday's constant and α_a and α_c are the anodic and cathodic transfer coefficients, respectively.

It is important to note that this equation also implies that η_{ct} is defined under the conditions that there are no mass transfer limitations, *ie* the concentrations of the electroactive species at the surface are identical or very close to the concentrations in the bulk.

The charge transfer resistance can be expressed as

$$R_{ct} = \left(\frac{\partial\eta}{\partial i}\right)_{i\to 0} = \frac{RT}{i_0(\alpha_a + \alpha_c)F}. \tag{3}$$

3.2. *Effect of mass transfer*

In reality, however, as current passes through an interface, a gradient in concentration of electroactive species will be created at the interface, leading to concentration polarization. Accordingly, mass transfer generally contributes to the interfacial overpotential and equation (1) should be replaced by:

$$\eta(t) = \eta_{ct}\left[1 - \exp\left(-\frac{t}{C_{dl}R_{ct}}\right)\right] + \eta_{mt}(t) \tag{4}$$

where $\eta_{mt}(t)$ is the overpotential due to mass transfer.

The mass transfer overpotential due to the concentration gradient of species i can be approximated by[6]

$$\eta_{mt,\,i}(t) = \left(\frac{RT}{\alpha_i F}\right)\ln\left(\frac{c_i(0,\,t)}{c_i^*}\right), \tag{5}$$

where α_i is the anodic or cathodic transference coefficient for the electrochemical reaction involving species i, c_i^* is the concentration of species i in the bulk phase, and $c_i(0, t)$ is the concentration of species i at the interface at a given time t.

When a constant current, I, is applied to an interface, the surface concentration of species i at any given time can be expressed as[7]

$$c_i(0,\,t) = c_i^* \pm \frac{2It_i(t)^{1/2}}{n_i FA(\pi D_i)^{1/2}}, \tag{6}$$

where D_i is the diffusion coefficient of species i, t_i is the transference number of species i, and n_i is the number of electrons transferred in the reaction involving species i. The use of a plus or minus sign depends on the nature of the electrochemical reaction. When an electrochemical reaction generates species i at an interface, a plus sign should be used

while a minus sign is appropriate for an electrochemical reaction which consumes species i at an interface. This is because the polarity of the overpotential increases the overpotential at the interface and hence diminishes the driving force for that electrochemical process.

Thus, the overpotential due to mass transfer of species i can be expressed in terms of the applied current as

$$\eta_{mt,i} = \left(\frac{RT}{\alpha_i F}\right) \ln\left[1 \pm \frac{2It_i t^{1/2}}{n_i F A c_i^* (\pi D_i)^{1/2}}\right]. \quad (7)$$

If the mass transport of more than one species contributes to the concentration overpotential, the total overpotential due to mass transfer will be the summation over all species:

$$\eta_{mt}(t) = \sum_i \eta_{mt,i}(t). \quad (8)$$

3.3. *Sequential current pulses and potential response*

Consider a solid-state electrochemical cell as depicted in Fig. 1a. The electrical response of the cell can be approximated by an equivalent circuit as shown in Fig. 1b, particularly when the current passing through the cell is reasonably small compared to the limiting current. When symmetric, sequential current pulses, as shown in Fig. 4, are applied to the cell, the corresponding potential response for each pulse ($0 < t \leqslant \tau_0$) can be described as

$$V_{1-2}(t) = \eta_{ct,1}\left[1 - \exp\left(-\frac{t}{\tau_1'}\right)\right] \pm \sum_i \frac{RT}{\alpha_i F} \ln\left[1 \pm \left(\frac{t}{\tau_{i,1}''}\right)^{1/2}\right] \quad (9)$$

$$V_{2-3} = IR_{ohmic} \quad (10)$$

$$V_{3-4}(t) = \eta_{ct,2}\left[1 - \exp\left(-\frac{t}{\tau_2'}\right)\right] \pm \sum_i \frac{RT}{\alpha_i F} \ln\left[1 \pm \left(\frac{t}{\tau_{i,2}''}\right)^{1/2}\right], \quad (11)$$

where the relaxation time associated with double layer charging at each interface can be expressed as

$$\tau_1' = C_{dl,1} R_{ct,1} = \left[\left(\frac{1}{\alpha_a + \alpha_c}\right)\left(\frac{RT}{F}\right)\frac{C_{dl}}{i_0}\right]_{\text{interface 1}} \quad (12)$$

$$\tau_2' = C_{dl,2} R_{ct,2} = \left[\left(\frac{1}{\alpha_a + \alpha_c}\right)\left(\frac{RT}{F}\right)\frac{C_{dl}}{i_0}\right]_{\text{interface 2}}, \quad (13)$$

respectively, and the transition time associated with mass transport of species i near each electrode surface can be defined as

$$(\tau_{i,1}'')^{1/2} = \left[\frac{n_i F A c_i^* (\pi D_i)^{1/2}}{2It_i}\right]_{\text{interface 1}} \quad (14)$$

$$(\tau_{i,2}'')^{1/2} = \left[\frac{n_i F A c_i^* (\pi D_i)^{1/2}}{2It_i}\right]_{\text{interface 2}}. \quad (15)$$

Clearly, the two time constants have very different characteristics. τ' is independent of the applied current and depends on double layer capacitance and exchange current density. On the other hand, τ'' depends on the applied current density, the diffusion coefficient, transference number, and the concentration of the electroactive species.

3.4. *Pulse width and error analysis*

Since the electrochemical response of an interface is strongly time-dependent, it is important to select the appropriate pulse width in order to minimize or eliminate complications due to mass transport and double layer charging. In other words, the duration of the current pulse should be long enough so that the current due to double layer charging is reasonably small and yet short enough so that the concentration of the electroactive species at the surface is reasonably close to the concentration in the bulk.

If the charge transfer overpotential at each applied current pulse, η_{ct}, is approximated to by the corresponding potential response taken at $t = \tau_0$,

$$\eta(\tau_0) = V_{1-2}(\tau_0), \quad (16)$$

then the relative error brought about by charging of the double layer and by mass transport near the electrode surface can be expressed as

$$\epsilon = \left|\frac{\eta_{ct} - \eta(\tau_0)}{\eta_{ct}}\right| = \left|\exp\left[-\frac{\tau_0}{\tau'}\right] \mp \left(\frac{1}{\eta_{ct}}\right)\sum_i \frac{RT}{\alpha_i F} \ln\left[1 \pm \left(\frac{\tau_0}{\tau_i''}\right)^{1/2}\right]\right|. \quad (17)$$

The first term on the right is due to charging or discharging of the double layer and the following terms are due to the mass transfer limitations. Three points are worth making: (i) because the first term is always positive and the following terms within the summation sign are all negative (by appropriate selection of the signs), the error introduced by double layer charging tends to cancel the errors introduced by mass transfer; (ii) the bipolar characteristics of the current pulse tend to cancel the error introduced by mass transport; and (iii) the transition time constant of mass transfer depends critically on the applied current density.

Shown in Fig. 5a are the normalized interfacial overpotentials as a function of normalized time. The interfacial overpotentials were normalized by the steady-state charge transfer overpotential whereas the time was normalized by τ', the double layer relaxation time constant. Specifically, Fig. 5b shows the normalized interfacial overpotentials as a function of time for interfaces with different time constants. Clearly, the interfacial potential approaches the steady-state charge transfer overpotential as time goes on (if the mass transfer is sufficiently fast). Consequently, the pulse width should be much longer than the double layer relaxation constant in order to minimize the error introduced by double layer charging.

Shown in Fig. 6 are the normalized overpotentials introduced by concentration polarization as a function of normalized time. The overpotentials were normalized by $(RT/\alpha_i F)$ whereas time was normal-

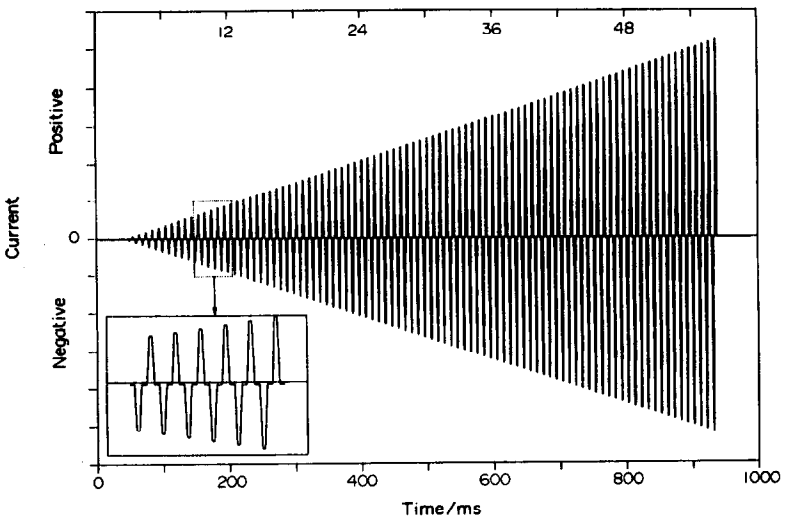

Fig. 4. A typical sequential, bipolar, square wave current pulses used to perturb a solid-state electrochemical cell for four probe polarization measurements.

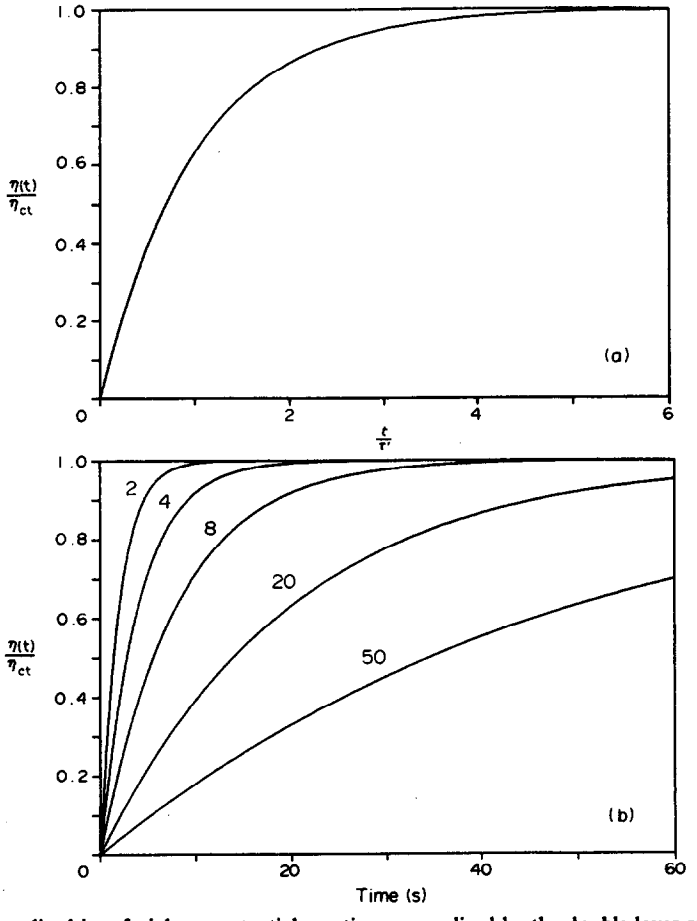

Fig. 5. (a) Normalized interfacial overpotentials vs. time, normalized by the double layer relaxation time constant; (b) normalized interfacial overpotentials vs. time for interfaces with a double layer relaxation time constant of 2, 4, 8, 20 and 50 ms.

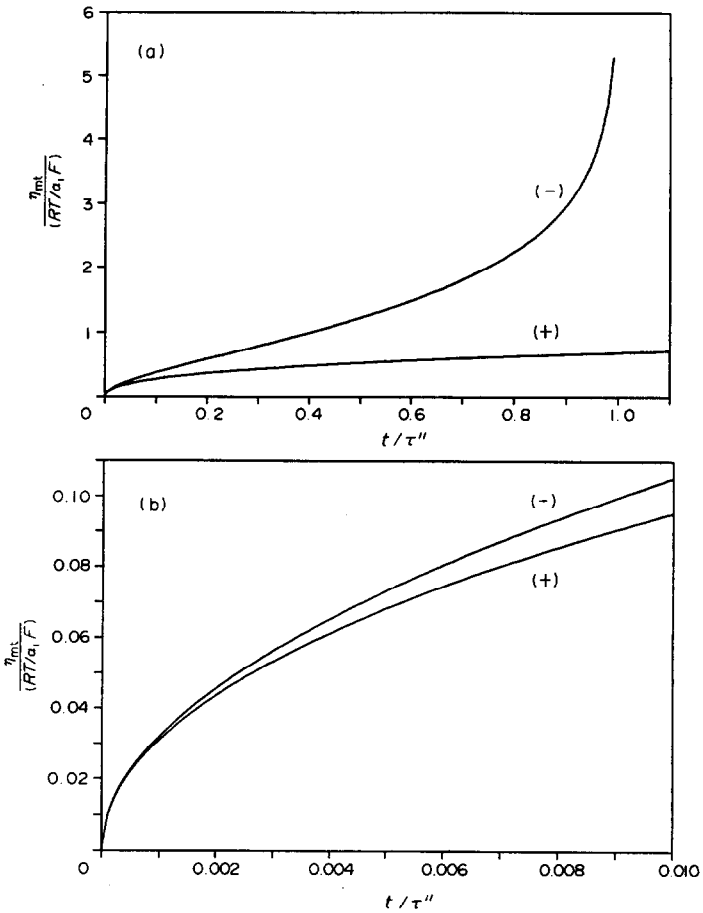

Fig. 6. Normalized mass-transfer overpotential vs. normalized time for: (a) the entire time domain; and (b) small ratios of t/τ''. The curve labeled with a (+) sign represents the case where an electroactive species is produced at the interface and the plus sign was used in the calculation. Similarly, the curve labeled with a (−) sign corresponds to the case where an electroactive species is consumed at the interface and the minus sign was used in the calculation.

ized by τ'', the transition time for mass transfer as defined by equations (14) and (15). Clearly, τ'' is directly influenced by the diffusion coefficient, the transference number and the concentration of the electroactive species as well as by the applied current density. Shown in Fig. 6a are the overpotentials due to mass transfer in the entire time domain and shown in Fig. 6b are the concentration overpotentials in the time range where the ratio of t/τ'' is relatively small. Clearly, the pulse width should be as small as possible in order to minimize the error introduced by mass transfer.

Shown in Fig. 7 are the combined effects of double layer charging and mass transfer on interfacial overpotential. Figure 7a shows the effect in the whole time domain. The effect of double layer charging was exaggerated by assuming the double layer relaxation time constant to be 40 s, much longer than experimentally observed values. The effect of mass transfer was also exaggerated by assuming the transition time constant for mass transfer to be 1000 s, much shorter than the experimentally observed values. Accordingly, the errors presented in the figure are much worse than the actual errors in an experiment. A more realistic case is shown in Fig. 7b, where the combined effect is illustrated for a time domain with $\tau' = 40\,\text{ms} \ll t \ll 1000\,\text{s} = \tau''$. Clearly, if the pause width is selected more than 200 ms and less than 2000 ms, the errors introduced by double layer charging and mass transfer are very small.

4. DETERMINATION OF TIME CONSTANT AND PULSE WIDTH

4.1. *Double layer relaxation time constant*

The relaxation time constant of a double layer can be readily determined by impedance spectroscopy. Shown in Fig. 8 are the impedance spectra of a solid oxide fuel cell as shown schematically in Fig. 3. The total impedance of the cell is shown in Fig. 8a, where at least two relaxation processes are observable. The introduction of four probes successfully separated the two interfaces so that the time constant for each interface could be determined separately. Shown in Fig. 8b is an impedance spectrum of the interface between the nickel cement electrode and the YSZ electrolyte measured at 1000°C in hydrogen. The relaxation time constant for hydrogen oxidation and

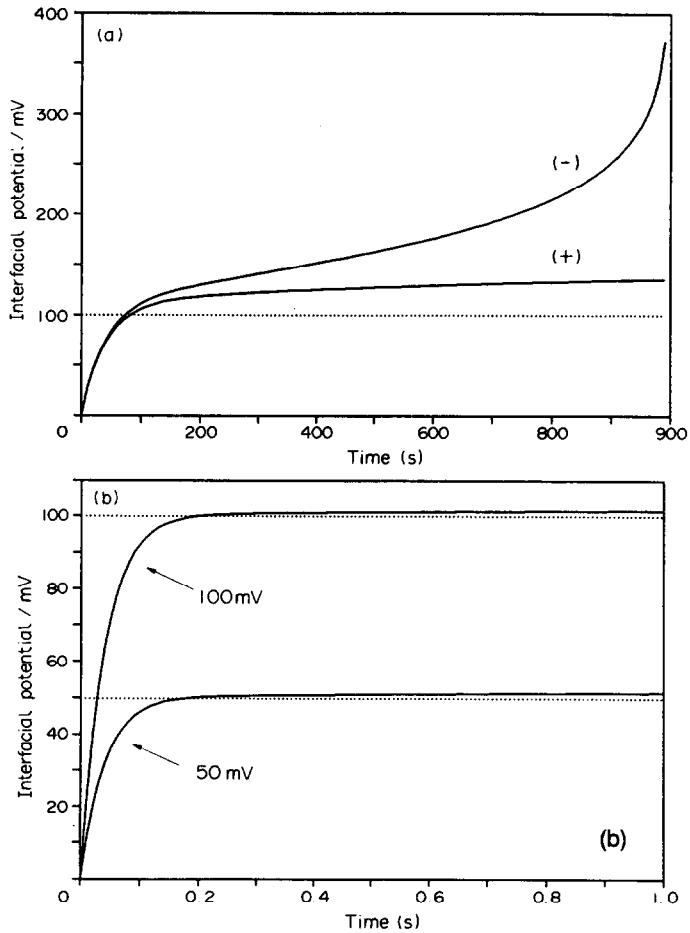

Fig. 7. The combined effects of double layer charging and mass transfer on the interfacial overpotentials: (a) for the entire time domain (assumed $T = 298$ K, $\alpha_i = 0.5$, $\tau' = 40$ s, $\tau'' = 1000$ s, and $\eta_{ct} = 100$ mV); and (b) for the region where $\tau' \ll t \ll \tau''$ (assumed $T = 298$ K, $\alpha_i = 0.5$, $\tau' = 40$ m, $\tau'' = 1000$ s and $\eta_{ct} = 50$ and 100 mV).

liberation under these conditions was in the order of 0.3 ms. Shown in Fig. 8c is an impedance spectrum of an interface between the LSM electrode and the YSZ electrolyte measured at 1000°C in air. The relaxation time constant for oxygen reduction was in the order of 12 ms.

Shown in Fig. 9 are some typical impedance spectra of the LSM/YSZ interface measured at 900°C in sample gases containing different partial pressures of oxygen. Clearly, the relaxation time constants for oxygen reduction and evolution were a function of partial pressure of oxygen, changing from 25 ms in oxygen to 35 ms in air and to about 80 ms in 1% oxygen balanced with N_2. In addition, comparison of Fig. 9 with Fig. 8c indicates that the kinetics of the processes slow down and the time constant increases as temperature decreases.

4.2. *Mass transfe transition time constant*

The relaxation time constant associated with mass transfer can be readily determined by chronopotentiometry. Figure 10 shows some typical discharge curves of Li/PEO/*srpe* cells at a constant discharge current density. First of all, the estimated relaxation time constants range from 1500 to 10,000 s, much longer than the relaxation time constants observed for double layer charging in a solid-state electrochemical device. In addition, the mass transfer transition time constant is a strong function of the applied current density. Clearly, as the current density increases, the time constant decreases. Furthermore, the time constant decreases as the operating temperature increases. This is because the transport properties are influenced exponentially by temperature. Accordingly, it is advisable to keep the applied current density, or the pulse height, as low as possible and to keep the operating temperature as high as possible to minimize mass transfer limitations.

4.3. *Pulse width*

Clearly, the time constant for double layer charging is in orders of magnitude smaller than that for mass transfer, particularly when the applied current density is relatively small and when the operating temperature is relatively high. In order to minimize the error introduced by mass transfer and by double layer charging, the pulse width should be kept a few times greater than the relaxation time of the double layer and much smaller than the transition time for

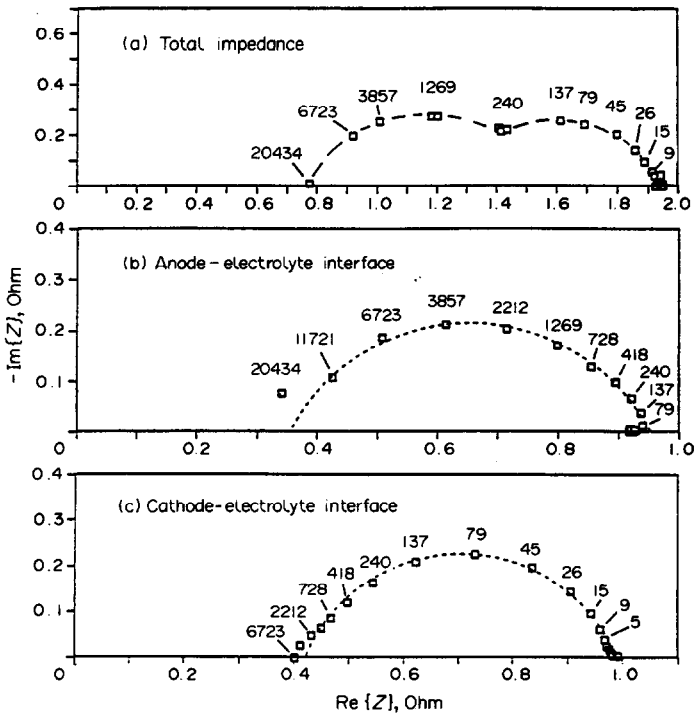

Fig. 8. Impedance spectra of a fuel cell (H_2 with 3% H_2O, Ni/YSZ/LSM, air) at 1000°C: (a) the total impedance of the cell; (b) the impedance of the anode–electrolyte interface; and (c) the impedance of the cathode–electrolyte interface. The numbers by the data points represent frequency in Hz. The working electrode area was 2.5 cm^2. The double layer relaxation time constants were about 0.3 ms for the anode–electrolyte interface and about 12 ms for the cathode–electrolyte interface.

mass transfer. The optimum pulse width can be estimated from minimization of equation[17].

5. APPLICATIONS

The application of four probe polarization techniques to the study of solid state electrochemical systems can be demonstrated below.

5.1. *Limiting factor to cell performance*

One of the unique advantages of four probe polarization techniques is the easiness and lack of ambiguity in identifying the limiting factor of cell performance. Consider an electrochemical cell as depicted in Fig. 2. When a current, either sequential pulses with appropriate pulse widths or a constant current, is applied to the cell, the ohmic potential

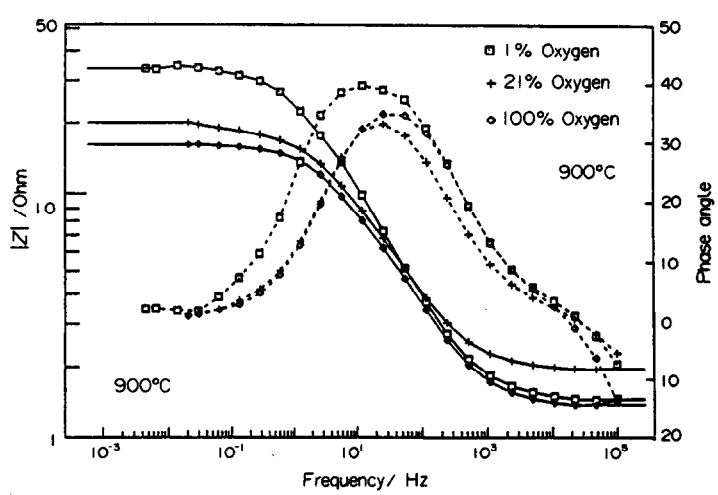

Fig. 9. Impedance spectra of an interface between $La_{0.89}Sr_{0.1}MnO_{3-x}$(LSM) and $(Y_3O_2)_{0.08}(ZrO_2)_{0.92}$ (YSZ) measured at 900°C. The double layer relaxation time constants are about 25 ms in oxygen, 35 ms in air and about 80 ms in 1% oxygen balanced with N_2.

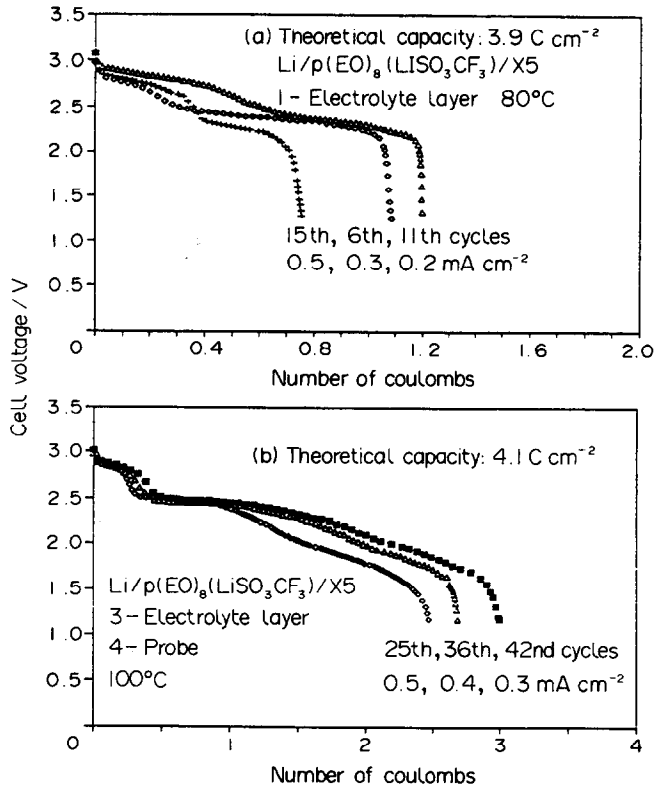

Fig. 10. Typical discharge curves of solid-state Li/p(EO)$_8$(LiSO$_3$CF$_3$)/X5 cells with different cell configurations: (a) the cell had a single electrolyte layer (as shown in Fig. 1) and was operated at 80°C. The mass-transfer transition time constants for the three curves were about 1500, 3500 and 6000 s, respectively; (b) the cell had three electrolyte layers (as shown in Fig. 2) and was operated at 100°C. The mass-transfer transition time constants for the three curves were about 5000, 6750 and 10,000 s, respectively.

drop across the electrolyte can be estimated as

$$V_{\text{ohmic}} = 3V_{2-3}. \tag{18}$$

The potential drop across the interface on the left, or the anodic overpotential of the cell, is given by

$$\eta_a = V_{1-2} - V_{2-3}, \tag{19}$$

while the potential drop across the interface on the right, or the cathodic overpotential of the cell, is given by

$$\eta_c = V_{3-4} - V_{2-3}. \tag{20}$$

Thus, the potential drop across the interfaces and across the electrolyte can be clearly separated.

Shown in Fig. 11a is the response of a Li/PEO/*srpe* cell (as shown in Fig. 2) to the sequential current pulses as shown in Fig. 4. The resistance of the electrolyte and the interfacial polarization resistances of the cell can be determined from the slopes of the polarization curves. The data presented in Fig. 11a clearly indicate that it is the positive electrode which limits the performance of the cell. Shown in Fig. 11b is a steady-state, four probe polarization measurement on the same cell when a constant current density of 0.3 mA cm^{-2} was continuously drawn from the cell. Although the resistance of each cell component varied during the course of discharge, the relative contribution of each component to the total polarization remained similar: the positive electrode is the limiting contribution to the overall polarization. Consequently, the performance of the positive electrode has to be improved in order to improve the performance of the cell effectively.

Activation parameters for the various components of the cell can be determined by making the same measurements over a range of temperatures. In Fig. 12, pulse polarization measurements were made on a four probe Li/aPEO/Li$_2$*X*1 cell from ambient to 70°C, and the resistances of the lithium–aPEO interface, aPEO electrolyte and composite positive electrode were determined over the temperature range as described above. In this case, the close similarity in the temperature dependence of the electrolyte and the positive electrode resistance indicates that the performance of the positive electrode is controlled by the relatively low conductivity of the electrolyte.

Shown in Fig. 13 are some *I*–*V* characteristics of a solid oxide fuel cell as shown in Fig. 3. The total overpotential of the cell was split into three contributions: (i) the potential drop across the electrolyte (*IR* drop); (ii) the anodic overpotential (across the anode–electrolyte interface); and (iii) the cathodic overpotential (across the cathode–electrolyte interface). For this specific cell, the ohmic drop across the electrolyte clearly contributes most to the overall polarization loss at high operating currents

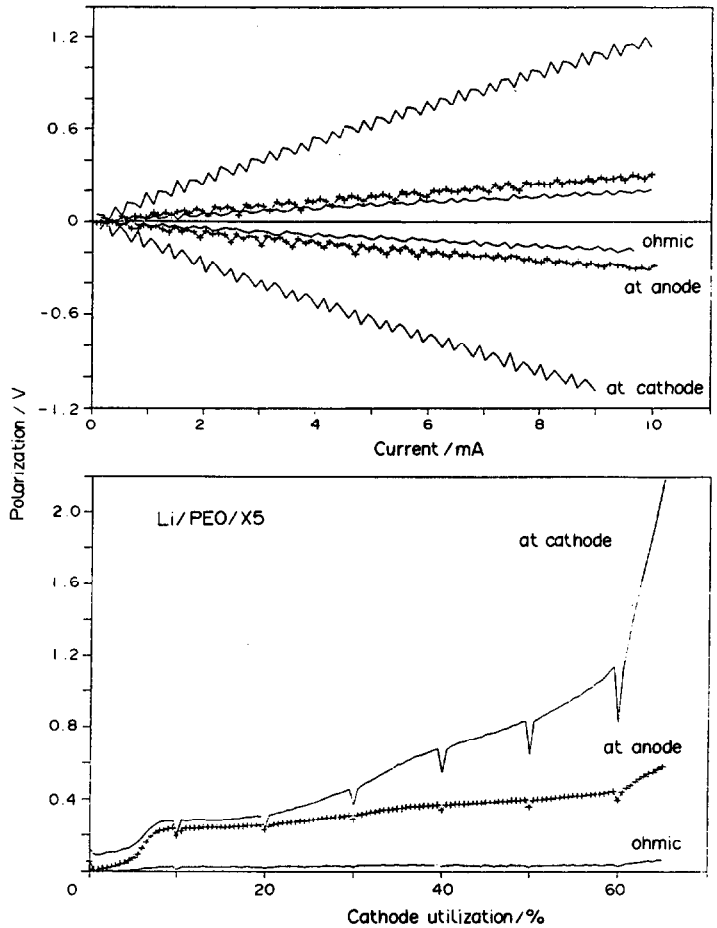

Fig. 11. Four probe polarization measurements on an Li/$p(EO)_8LiN(SO_2CF_3)_2/X5$ cell at 100°C: (a) potential drop across each cell component when the cell was perturbed by current pulses with pulse width of 0.3 s; and (b) potential drop across each cell component when a constant current density of 0.3 mA cm^{-2} was drawn from the cell.

(above 500 mA). In this case, the improvement in the electrolyte conductivity will most effectively improve the overall cell performance. At low operating currents (below 100 mA), however, each component has a similar contribution to the overall polarization loss.

The successful separation in performance of each cell component clearly identifies the rate limiting

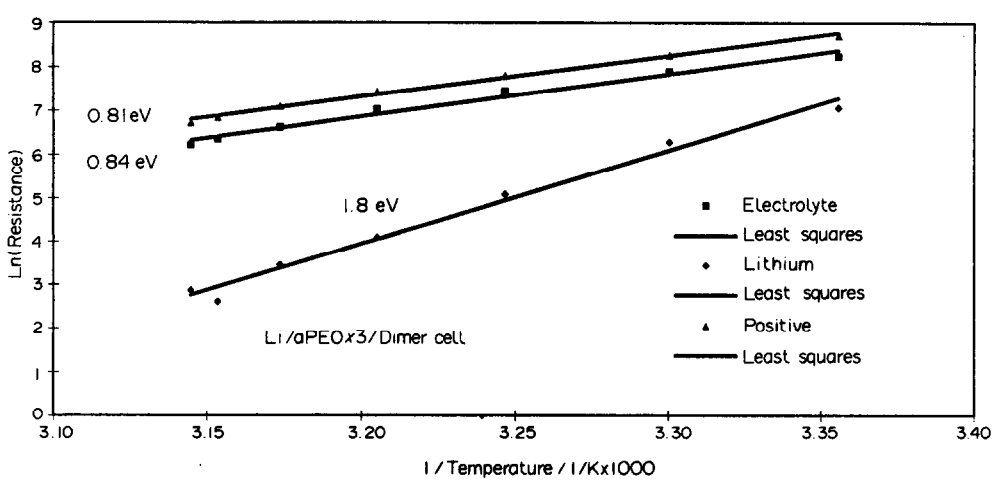

Fig. 12. Arrhenius plot of the resistances of the electrolyte and electrode interfaces in an Li/aPEO$x3/Li_2X1$ cell, as determined from four probe pulse polarization measurements.

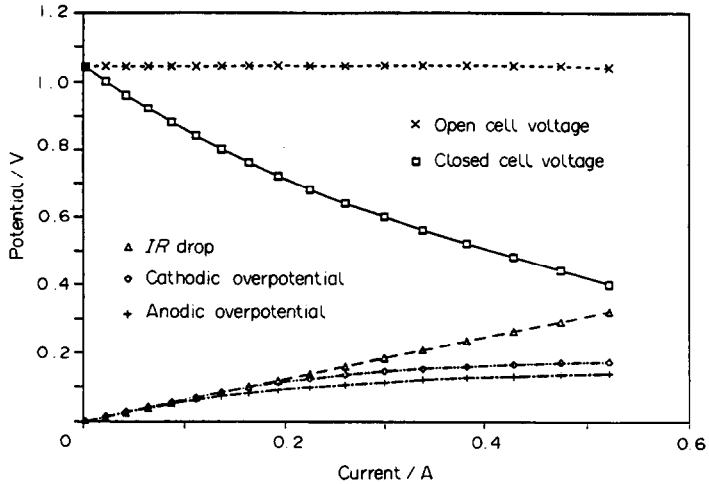

Fig. 13. Current–potential characteristics of a solid oxide fuel cell. The total overpotentials of the cell at various operating current densities were divided into three contributions: IR drop across the electrolyte, the anodic overpotential, and the cathodic overpotential. The working electrode area was 2.5 cm^2.

factor of a specific cell and hence provides valuable information for most effective improvement of cell performance.

5.2. *Electrolyte conductivity*

The conductivity of the electrolyte can be readily estimated from the relationship between the applied current and the potential drop across the electrolyte, V_{2-3}.

5.3. *Electrode kinetics*

If the error introduced by mass transfer and double layer charging can be kept reasonably small through experimental design and through careful selection of pulse width, the kinetic behavior of the electrode can be further studied in detail. Once the charge transfer overpotential is determined at each applied current, various kinetic parameters can be determined using equation (2).

For example, shown in Fig. 14 is the room temperature polarization response of a positive electrode in a Li/gelled PEO/$X$1 cell as determined from four probe pulse measurements. In this case, Tafel behavior of the positive electrode is cleanly separated from the overall cell response. The polarization response of the positive electrode can be fitted to equation (2) with an additional iR term for ohmic drop within the composite positive electrode. The exchange current and ohmic drop in the positive electrode can then be calculated by a non-linear curve fit of the data as shown in Fig. 13.

5.4. *Other applications*

With known kinetic information, other transport properties of the electrolyte or the electrode can be studied as well.

6. CONCLUSIONS

A number of solid-state batteries based on redox polymerization electrodes and solid oxide fuel cells

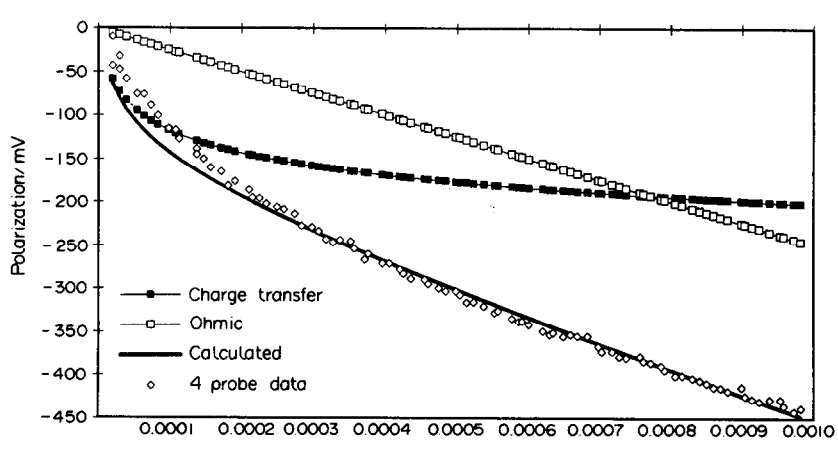

Fig. 14. Positive electrode polarization in a Li/PEO (plasticized)/$X$1 cell as determined from four probe measurements; calculated fit corresponds to $\alpha = 0.35$, $R_{ohmic} = 250\,\Omega$ and $i_0 = 4 \times 10^{-6}$.

have been successfully studied using four probe polarization techniques. These techniques are particularly useful for quick diagnosis of an electrochemical cell for performance optimization or for identifying the rate-limiting component of a system. In addition, careful design of experimental cell and appropriate selection of pulse width can further lead to fundamental studies of electrode kinetics and transport properties.

Acknowledgement—This research was supported by the Assistant Secretary for Conservation and Renewable Energy, Deputy Assistant Secretary for Utility Technologies, Office of Energy Management, Advanced Utility Concepts Division of the U.S. Department of Energy under Contract No. DE-AC03-76SF00098.

REFERENCES

1. M. Liu, S. J. Visco and L. C. De Jonghe, *J. electrochem. Soc.* **138**, 1891 (1991).
2. M. Liu, S. J. Visco and L. C. De Jonghe, *J. electrochem. Soc.* **138**, 1896 (1991).
3. S. J. Visco, M. Liu and L. C. De Jonghe, *Mol. Cryst. Liq. Cryst.* **190**, 185 (1990).
4. M. Liu and A. Khandkar, *Solid State Ionics* **52**, 3 (1992).
5. S. J. Visco and M. Liu, *J. appl. Electrochem.* **22**, 307 (1992).
6. J. Goodisman, *Electrochemistry: Theoretical Foundations*. Wiley, New York (1987).
7. A. J. Bard and L. R. Faulkner, *Electrochemical Methods, Fundamentals and Applications*. Wiley, New York (1980).